Taylor & Francis
Taylor & Francis Group

ORIGINAL RESEARCH

🔓 OPEN ACCESS Check for updates

S100A10 promotes cancer metastasis via recruitment of MDSCs within the lungs

Juan Li[a,b]*, Can Zhou[c]*, Xiaoqian Gao[a,b], Tan Tan[d], Miao Zhang[a,b], Yazhao Li[a,b], He Chen[a,b], Ruiqi Wang[a,b], Bo Wang[a,b], Jie Liu[a,b], and Peijun Liu [iD][a,b]

[a]Center for Translational Medicine, the First Affiliated Hospital of Xi'an Jiaotong University, Xi'an, Shaanxi, China; [b]Key Laboratory for Tumor Precision Medicine of Shaanxi Province, the First Affiliated Hospital of Xi'an Jiaotong University, Xi'an, Shaanxi, China; [c]Department of Breast Surgery, the First Affiliated Hospital of Xi'an Jiaotong University, Xi'an, Shaanxi, China; [d]Center for Precision Medicine, the First People's Hospital of Chenzhou, Chenzhou, Hunan, China

ABSTRACT

Tumor-derived exosomes bind to organ resident cells, activating S100 molecules during the remodeling of the local immune microenvironment. However, little is known regarding how organ resident cell S100A10 mediates cancer metastatic progression. Here, we provided evidence that S100A10 plays an important role in regulating the lung immune microenvironment and cancer metastasis. S100A10-deficient mice reduced cancer metastasis in the lung. Furthermore, the activation of S100A10 within lung fibroblasts via tumor-derived exosomes increased the expression of CXCL1 and CXCL8 chemokines, accompanied by the myeloid-derived suppressor cells (MDSCs) recruitment. S100A10 inhibitors such as 1-Substituted-4-Aroyl-3-hydroxy-5-Phenyl-1 H-5-pyrrol-2(5 H)-ones inhibit lung metastasis in vivo. Our findings highlight the crucial role of S100A10 in driving MDSC recruitment in order to remodel the lung immune microenvironment and provide potential therapeutic targets to block cancer metastasis to the lung.

Introduction

Cancer metastasis is the primary cause of death in cancer patients. Within this local microenvironment of distant organs, immune cells and fibroblasts are known to regulate immune suppression vital for primary cancer cell metastasis.[1] Primary tumor-derived secreted molecular (TDSFs) and extracellular vesicles (EVs) induce bone marrow-derived cells (BMDCs) to accumulate in metastatic organs.[2,3] These BMDCs interact with resident stromal cells and the extracellular matrix of distinct organs to promote the formation of an immunosuppressive microenvironment.[4] The interaction mechanisms between primary tumors and distinct organs that initiate metastasis are still unclear and require more in-depth study.

Different BMDC types have demonstrated the ability to remodel metastatic organ environment. Studies have also shown that myeloid-derived suppressor cells (MDSCs) play an important role in cancer metastasis.[5] MDSCs can be recruited into the local immune microenvironment by chemokines, including CCL2, CXCL1, CXCL2, CXCL5, CXCL8 and CCL26[6]. MDSCs affect the immune microenvironment and extracellular matrix (ECM) during cancer metastasis.[5–7] However, how host stromal cells in distinct organs trigger MDSCs recruitment to remodel the local immune microenvironment are unclear. Fibroblasts are one of the most abundant stromal cell populations in distant tissue. In primary tumors, fibroblasts enhance tumor invasion via ECM remodeling,

promoting cancer-associated inflammation and supporting immune cell activation.[8,9] Additionally, whether fibroblasts could promote cancer metastasis by modifying the local immune microenvironment in distant organs still needs to be studied.

S100A10, a plasminogen receptor, activates the plasminogen pathway by binding to the cell surface receptor annexin 2.[10] In cancer cells, upregulation of S100A10 has been found to increase plasmin, promote ECM degradation, and enhance cell growth and migration.[11,12] Furthermore, S100A10 has been reported to affect the trafficking of membrane proteins, including the serotonin 5-HT1B receptor,[13] channel proteins TRPV5/TRPV6[14] and sodium channel protein Nav1.8.[15] S100A10-Annexin2 heterotetramer also mediates the stemness and chemoresistance of breast cancer. Paclitaxel increases the expression of S100A10, forming a complex with the histone demethylase KDM6A and the histone chaperone SPT6. This large complex is recruited to the OCT4 binding sites, facilitating the transcription of stem cell marker genes.[16] Recent studies have shown that tumor-derived exosomes bind organ stromal cells and activate Src and S100 molecules in distant tissue microenvironments.[17] However, the effect of S100A10 in resident stromal cells on tumor progression remains unclear. Here, we focus on how resident stromal cell S100A10 contributes to cancer metastasis and the remodeling of the local immune microenvironment. In this study, we constructed conventional S100A10 knockout mice to study the

effects of lung resident cell S100A10 on the remodeling of the local immune microenvironment and cancer metastasis *in vivo*. We found that S100A10 in lung fibroblasts activates chemokine expression and promotes MDSC recruitment within the lung immune microenvironment, thereby facilitating cancer metastasis.

Materials and methods

Mice models

Conventional C57BL/6 S100a10 knockout mice were obtained from the Saiye Model Animal Research Center. They were constructed using CRISPR/CAS9 techniques. The Genotyping Strategy is shown in Supplement Figure 1. All animal experiments were carried out according to a protocol approved by the Ethics Committee and the Institutional Animal Care and Use Committee of Xi'an Jiaotong University. The animal ethical approval number is XJTU1AF2024LSK-2023-091. In our study, all mice were of the same sex and age (range between 6 and 10 weeks).

Orthotopic and tail-vein tumor models

Luciferase or GFP-labeled B16/F10 melanoma cells (5×10^5) were administered intradermally in the flank of the mice. At 10 d, the tumor-bearing mice underwent surgical excision and continuous cultivation. Twenty-eight days after surgery, lung metastasis of the orthotopical tumor was monitored via bioluminescent imaging.

The B16/F10$^{LUC/GFP}$ (2×10^5) and E0771^{GFP} (5×10^5) injections were resuspended in PBS and injected into the tail-vein of C57BL/6 mice. At 12 d, the mice were sacrificed under anaesthetic, and tumor metastatic nodules in the lungs were evaluated via bioluminescent and fluorescent imaging, flow cytometry analysis and IHC/IF staining.

Adeno-associated virus 6 lung infection

Adeno-associated virus 6 encoding S100A10 (AAV6-S100A10) and AAV6-empty vector (AAV6-NC) were purchased from ViGene Biotech (Guangzhou, China). AAV6-S100A10 contained the fibroblast-specific promoter FSP1 that specifically induced the expression of S100A10 in lung fibroblast. Then, under anesthesia, every mouse was infected with 40ul of AAV6 (10^{11} genomic copies) by intratracheal instillation. Mice were rested for 3 weeks after infection in order to allow for rescue S100A10 expression in lung fibroblast of KO mice.

Depletion of MDSCs

Anti-Gr-1 Abs (BE0075, BioXcell) or isotype control (BE0090, BioXcell) was injected into the tail-vein of WT and KO mice at 200 μg/mouse the day before the B16/F10^{LUC} were implanted. Subsequently, Gr-1 Abs or isotype control was injected every 3 d into tail vein of WT and KO mice until mice were euthanized.

Isolation and application of tumor exosomes

B16/F10 cells and E0771 cells were cultured using RPMI-1640 or DMEM medium for 48 h, after which the medium was collected and centrifuged at 1500 rpm for 5 min. The supernatant was collected and centrifuged at 3000 rpm for 20 min. Next, the cell debris was removed, and the supernatant was filtered using a 0.2 mm filter (Pall Corporation). The collected medium was ultracentrifuged at 100,000 g for 90 min at 4°C, and the supernatant was discarded. Pelleted exosomes were resuspended in PBS, and protein content was quantified via the BCA method. Then, we verified the concentration and particle size of exosomes via nanometer particle size meter (RuiXin, Nanocoulter I).

For in vivo induction of pre-metastatic microenvironment formation, 10 μg of exosomes in 50 μl of PBS were injected into the mice's tail vein every 2 d. After 14 consecutive injections, the lungs were collected, and frozen sections were made. For in vivo exosome tracking experiments, purified exosomes were labeled with PKH26 red dye (Sigma). The labeled exosomes were washed, collected by ultracentrifugation, and resuspended in PBS. The labeled exosomes (10 μg) were then injected into the tail vein of the mice. One day after exosome injection, lung tissues were analyzed via immunofluorescence.

T-cell suppression assay

Isolation of Gr-1$^+$Ly-6 G$^+$ MDSCs, from the lung of WT and KO mice was performed. The MDSCs were isolated using a myeloid-derived suppressor cell isolation kit following the manufacturer's standard protocol (Miltenyi Biotec, 130-094-538).

The CFSE-labeled T cells and MDSCs were co-cultured in a 24-well plate. MDSCs and T cells were cultured at ratios of 1:4. The number of T cells was defined as 100,000 cells per well. T cells were then stimulated using 1 μg/ml anti-CD3 (BD Biosciences) and 2 μg/ml anti-CD28 (BD Biosciences) and incubated at 37°C for 72 h. Cell proliferation was measured using CFSE dilution and flow cytometry.

Flow cytometry

The single-cell lung suspensions were stained using antibodies targeting CD4$^+$ and CD8$^+$ T lymphocytes (CD3$^+$CD4$^+$ and CD3$^+$CD8$^+$), B cells (CD3$^+$CD19$^+$), macrophages (CD11b$^+$F4/80$^+$), dendritic cells (CD11c$^+$MHCII$^+$), MDSCs (CD11b$^+$Gr-1$^+$), M-MDSCs (CD11b$^+$Ly6C$^+$), PMN-MDSCs (CD11b$^+$Ly6G$^+$) and NK cells (CD3$^-$NK1.1$^+$). The analyses were performed using a CanoII flow cytometer (BD) or Novocyte flow cytometer (Agilent). The antibodies were purchased from the BD Pharmingen TM or Bioleng.

In vitro differentiation of MDSCs from murine bone marrow

Murine bone marrow cells were isolated and cultured for 4 d in RPMI-1640 medium with 10% FBS, 10 mM HEPES, 1 mM sodium pyruvate, 1 mM MEM non-essential amino acids,
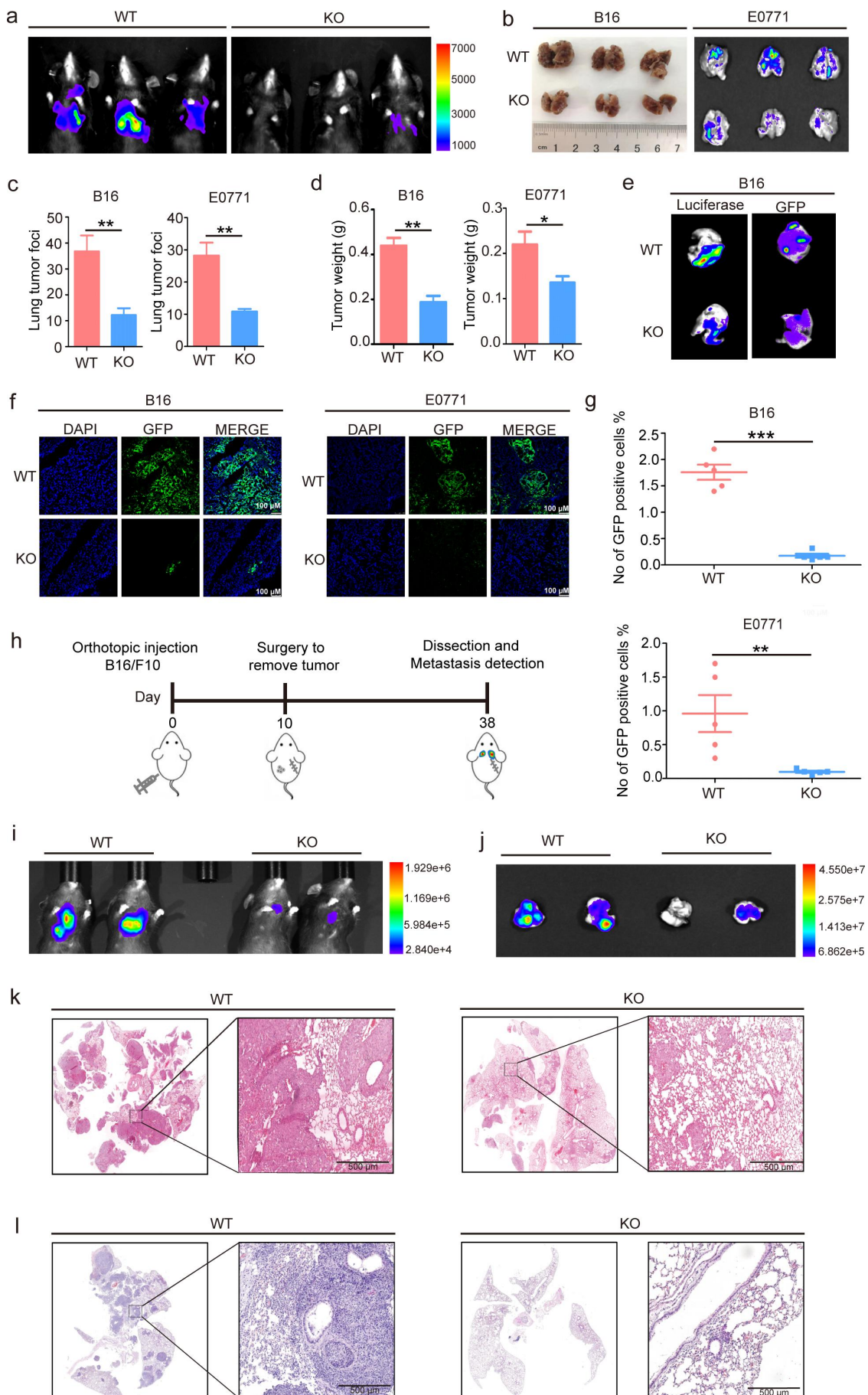
Figure 1. S100A10 deficiency prevents lung metastasis. a) Representative images of B16/F10 lung metastasis in S100A10-deficient or WT mice via luciferase bioluminescence in vivo. b) Representative images of B16/F10 and E0771 lung metastasis nodules in S100A10-deficient or WT mice. c) Quantitation of B16/F10 and

50 μM β-mercaptoethanol, 1% penicillin/streptomycin, 40 ng/mL GM-CSF (PeproTech 315–03), and 40ng/mL IL-6 (PeproTech 216–16).

Generation of murine bone marrow chimeras

The recipient mice were lethally irradiated to ablate their hematopoietic stem cells. Bone marrow (BM) cell suspensions were prepared from donor mice. 1×10^7 BM was transplanted into recipient mice. Recombinant mice were then treated with neomycin for 3 weeks to limit the risk of infection and were monitored regularly. After 3 weeks, flow cytometry was used to detect the bone marrow cell subtypes of the recombinant mice in order to evaluate the recombinant efficiency.

In vitro migration assay

We used a chemotaxis chamber (Corning 3422) to evaluate the effect of cell-conditioned media on the migration of MDSCs. A 100 μl MDSCs cell suspension (5×10^5 cells) aliquot was seeded into the upper wells. In the lower wells, 50 ng/ml recombinant mouse S100A10 protein (ProSpec pro-2252) or NIH3T3 cell stimulated by tumor exosome conditioned media were placed. An 8 μm pore size polycarbonate filter separated the upper and lower wells. After incubation for 3 h at 37°C with 5% CO_2, the number of MDSCs that migrated to the lower wells was counted.

Immunofluorescence

The frozen tissue section was fixed using 4% paraformaldehyde and permeabilized with 0.1% Triton-X100 for 10 min. The sections were incubated with primary antibodies targeted against S100A4 (Proteintech 16,105–1-AP), Fibronectin (Santa Cruz sc-8422 1:100), Gr-1 (CST#31462 1:200), and Flag (Sigma Aldrich F1804 1:100) overnight at 4°C. The secondary antibodies, labeled with Alexa Fluor 488 (Invitrogen) and Alexa Fluor 546 (Invitrogen) were photo-imaged using a fluorescent microscope (Leica TCS SP5 II, Germany).

Statistical analysis

Each experiment was repeated at least three times. Results are expressed as mean ± SD or SEM as indicated. Statistical analysis was performed using GraphPad Prism 5 and presented in the following manners: $*p < 0.05$, $**p < 0.01$ and $***p < 0.001$.

Results

S100A10 deficiency prevents lung metastasis

Recent studies have shown that tumor-derived exosomes bind to organ stromal cells and activate S100A10 in the lung microenvironment.[17] In this study, we tail vein inoculated S100A10$^{-/-}$ mice with B16/F10$^{LUC/GFP}$ melanoma cells and E0771^{GFP} breast cancer cells, then observed cancer metastasis in order to study the role of organ resident cell S100A10 during tumor progression. A detailed construction of the S100A10 deficiency mice is shown in Supplemental Figure 1. Our results found that S100A10$^{-/-}$ (KO) mice revealed a significant reduction in lung metastasis compared to S100A10$^{+/+}$ wild-type (WT) mice (Figure 1a,b). We observed that S100A10 deficiency inhibited the number of metastatic nodules and thus decreased lung-metastasis tissue weight compared to WT mice (Figure 1c,d). In vitro observation of lung tissue showed that luciferase or GFP labeled B16/F10 cells from the lungs of KO mice are less than those of WT mice (Figure 1e). The immunofluorescence and flow cytometry results showed that B16/F10^{GFP} and E0771^{GFP} cells in WT mice were higher than in KO mice (Figure 1f,g).

To further study the role of organ resident S100A10 during lung metastasis of in situ tumor, we inoculated the mice with B16/F10^{LUC} via subcutaneous injection, allowing the cell to form a tumor. At 10 d, the tumor-bearing mice underwent surgical excision and continuous cultivation. Twenty-eight days after surgery, lung metastasis of the orthotopic tumor was monitored using bioluminescent imaging (Figure 1h). Compared to WT mice, KO mice had fewer metastases within the lung tissue (Figure 1i,j). The HE staining of whole lung tissue verified that S100A10 deficiency decreased the number of metastatic nodules (Figure 1k,l). Together, these observations suggest that host S100A10 contributes to lung metastasis of tumor.

S100A10 deficiency prevents the establishment of pre-metastatic microenvironment

The pre-metastatic microenvironment supports a favorable local microenvironment for the primary tumor metastasis. We used tumor-derived exosomes to induce pre-metastatic microenvironment formation within the lung of WT and KO mice (Figure 2a). We isolated exosomes from the B16/F10 and E0771 cells. We verified exosomes via nanometer particle size analysis and demonstrated the expression of exosome surface markers (Fig. S2). TIMP, S100A8, S100A9, and fibronectin play critical roles during pre-metastatic microenvironment formation.[18–21] We found that TIMP, S100A8, and

---

E0771 tumor cell focia within the lung tissue ($n = 6$ individual mice in each group, $**p < 0.01$). d) Quantitation of B16/F10 and E0771 metastasis lung weight ($n = 6$ individual mice in each group, $**p < 0.01$, $*p < 0.05$). e) Representative images of B16/F10 lung metastasis tissue in WT or KO mice via luciferase bioluminescence and GFP-labeled fluorescence. f) Immunofluorescent analysis S100A10-deficient or WT mice lung sections after GFP-labeled B16/F10 and E0771 inoculation (blue-DAPI, green-GFP, Scale bar, 100 μm). g) The percentage of GFP-positive B16/F10 and E0771 cells in the lung tissue of WT or KO mice detected by flow cytometry ($n = 5$ individual mice in each group, $***p < 0.001$, $**p < 0.01$). h) Schematic diagram for the lung metastasis of the in situ tumor. i) Representative luciferase bioluminescence images of B16/F10 lung metastasis from in situ S100A10-deficient or WT mice. j) Representative images of B16/F10 lung metastasis tissue from in situ S100A10-deficient or WT mice via luciferase bioluminescence. k) H&E-stained lung sections of S100A10-deficient or WT mice after tail-vein inoculation of B16/F10 cell. l) H&E-stained lung sections of KO or WT mice after subcutaneous injection of B16/F10 cell.
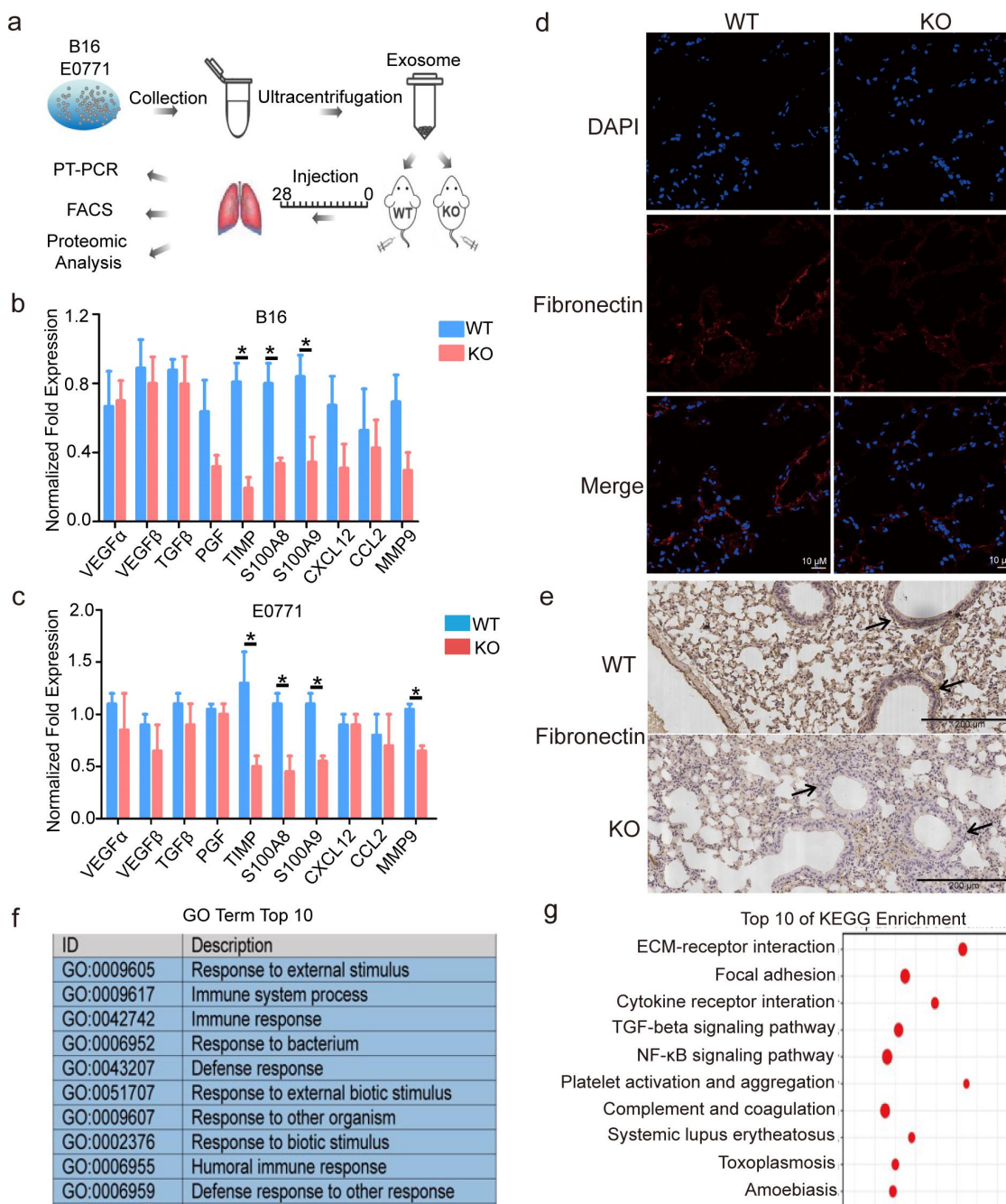
Figure 2. S100A10 deficiency prevents lung pre-metastatic microenvironment formation. a) Schematic diagram for the tumor-derived exosome induced formation of the pre-metastatic microenvironment. 10 μg of B16/F10 and E0771-derived exosomes in 50 μl of PBS were intravenously injected into the tail vein of S100A10-deficient or WT mice every 2 d. Pre-metastatic microenvironment formation in the lungs of mice after 28 d. b and c) Pro-metastatic gene expression in the lungs of S100A10-deficient or WT mice after B16/F10-derived exosome b) and E0771-derived exosomes c) induction was quantified by qPCR. d and e) Immunofluorescent analysis of lung tissue sections d) and IHC stained lung tissue sections e) of the fibronectin expression of S100A10-deficient mice or WT mice. f) Top 10 biological processes with enrichment of different expression gene sets in S100A10-deficient or WT mice lungs by GO analysis (n = 3 individual mice in each group). g) Top 10 signaling pathways with enrichment of different expression gene sets in S100A10-deficient or WT mice lungs by KEGG analysis (n = 3 individual mice in each group).

S100A9 expression in the lungs of S100A10 KO mice were significantly reduced compared to the lung of WT mice (Figure 2b,c). The IF and IHC results revealed that fibronectin expression was down-regulated in the pre-metastatic microenvironment of S100A10 KO mice (Figure 2d,e). To further evaluate the effect of S100A10 deletion on pre-metastatic microenvironment formation of the lungs, transcriptome sequencing was performed on lung tissue from S100A10 KO and WT mice. We found that the biological function of the differentially expressed genes was focused on the immune response and the external stimulus (Figure 2f). The KEGG enrichment showed that S100A10 deficiency affected the ECM–receptor interaction, cytokine receptor interaction, and TGF-β or NF-κB signaling pathway (Figure 2g). Thus, S100A10 deficiency suppresses pre-metastatic microenvironment establishment within the lungs.
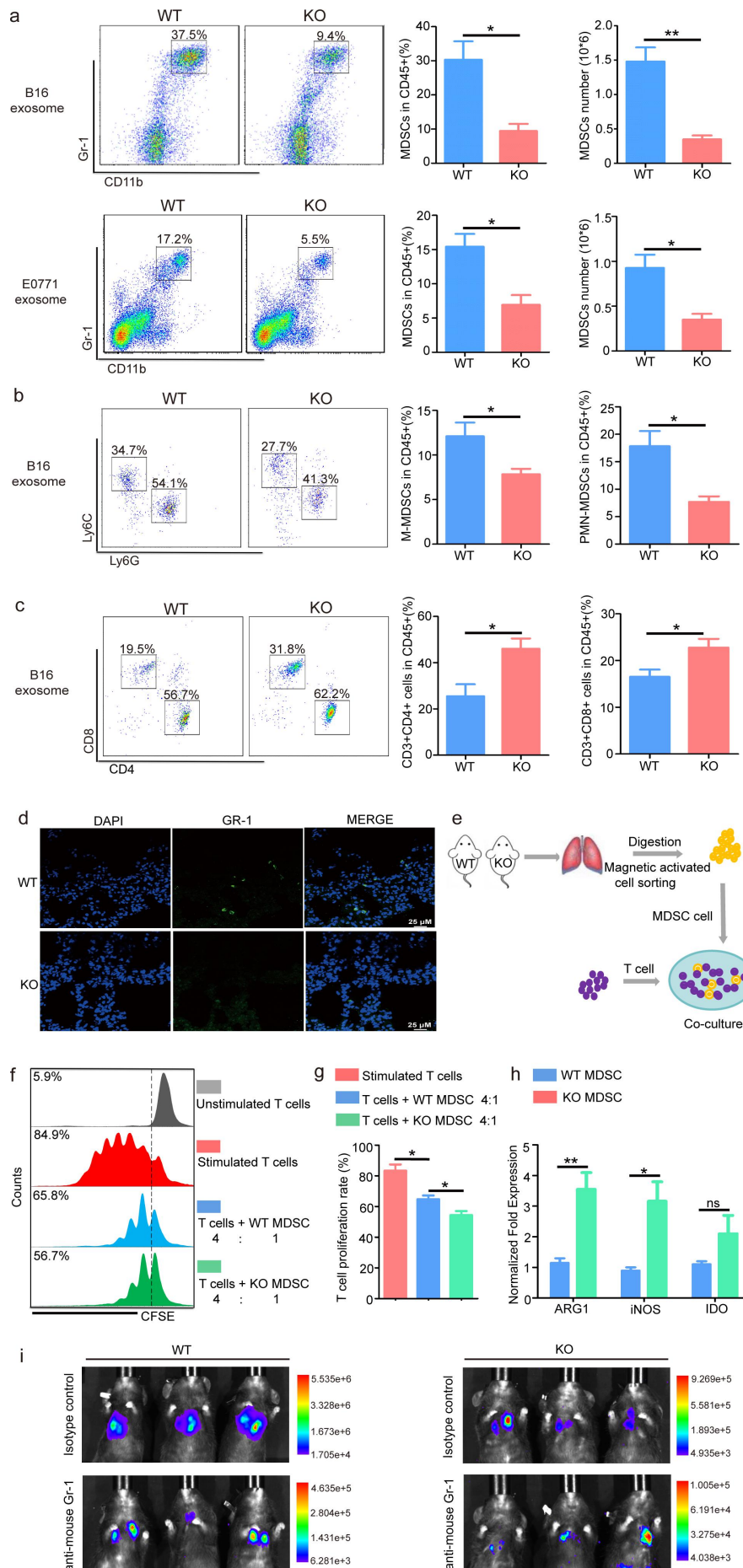
Figure 3. S100A10 deficiency inhibits MDSCs recruitment to the lung pre-metastatic microenvironment. a) The proportion of MDSCs in the lungs of KO or WT mice after B16/F10 or E0771-derived exosome inoculation was measured via flow cytometry ($n = 6$ individual mice in each group, $*p < 0.05$, $**p < 0.01$). b) The proportion of PMN-

S100A10 deficiency suppresses MDSCs recruitment to the lung metastatic microenvironment

To further assess which S100A10 host cell has the effect of promoting cancer metastasis, we carried out the bone marrow (BM) adoptive transfer experiments (Fig. S3a). The first group of chimeras is the donor BM of CD45.2 subtype S100A10 KO or WT mice and recipient mice of CD45.1 subtype WT mice. The chimeras were subsequently subjected to tail vein injections with B16/F10 cells. Bright-field observation and HE staining of whole lung tissue showed that mice adoptive transfer of KO mice BM had fewer metastatic nodules than those adoptive transfer of WT mice BM (Figure S3b-d). The second group of chimers is donor BM of CD45.1 subtype WT mice and recipient mice of CD45.2 subtype S100A10 KO or WT mice. The results showed that recipient mice S100A10 KO mice had significantly reduced metastatic nodules compared to recipient mice S100A10 WT mice (Figure S3e-g). These results demonstrate that S100A10 deficiency in the host tissue or immune cells all altered lung metastatic in S100A10 KO mice. However, the absence of S100A10 in the host tissue has a more significant effect on cancer metastasis.

Next, we analyzed the number of immune cells in the pre-metastatic microenvironment of S100A10 KO and WT mice after tumor-derived inoculation. CD11b$^+$Gr-1$^+$ MDSCs in the pre-metastatic lungs of KO mice were significantly decreased compared to S100A10 WT (Figure 3a). We further found that the percentage of Ly6G$^+$Ly6C^{low} PMN-MDSCs and Ly6G$^-$Ly6C^{high} M-MDSCs in the pre-metastatic lungs of KO mice is decreased compared to WT mice (Figure 3b). Furthermore, the number of CD3$^+$CD4$^+$ or CD3$^+$CD8$^+$ T cells in the pre-metastatic lungs of KO mice is increased (Figure 3c). The gating strategy for Figure 3b is shown in Supplemental Figure 4. The IF results showed that the number of MDSCs within the pre-metastatic lung of S100A10 KO mice was less than that of the WT mice (Figure 3d). CD11b$^+$F4/80$^+$ macrophage cells, CD11C$^+$MHCII$^+$ DC cells, and CD3$^-$NK1.1$^+$NK cells in the pre-metastatic lungs of S100A10 KO mice revealed no difference compared to WT mice (Fig. S5a-c). However, S100A10 knockout did not affect CD11b$^+$Gr-1$^+$ MDSCs or other immune cell numbers in the lymph glands or bone marrow (Figure S5d-h).

MDSCs exert immunosuppressive effects by targeting T cells. To examine the direct impact of MDSCs from S100A10 KO and WT mice lung metastatic microenvironment on effector T cells, we pre-treated T cells with anti-CD3 and anti-CD28 prior to co-culturing with lung MDSCs of WT and KO mice (Figure 3e). Compared to the S100A10$^{+/+}$ MDSCs, S100A10$^{-/-}$ MDSCs had increased capacity to inhibit T-cell proliferation

(Figures 3f,g). The expression of immuno-suppressive genes of S100A10$^{-/-}$ MDSCs, including ARG1 and iNOS, was higher than that of S100A10$^{+/+}$ MDSCs (Figure 3h). Furthermore, we determined whether down-regulated MDSCs infiltration is the main reason of the reduced tumor metastasis of S100A10 KO mice. We employed anti-Gr-1 neutralizing antibody to deplete MDSCs both in S100A10 KO and WT mice. We found that S100A10 WT and KO mice have the same of tumor metastasis burden in lung when deplete MDSCs (Figure 3i). These data suggest that S100A10 participates in MDSCs recruitment required for lung metastasis.

S100A10 deficiency of fibroblasts inhibits the activation of chemokines induced by exosomes and the migration of myeloid lineage

To understand the underlying mechanisms of impaired MDSCs recruitment in the pre-metastatic lungs of S100A10 KO mice after tumor-derived exosome stimulus, we first traced the location of the tumor-derived exosomes in the lung. Next, the B16/F10-derived exosomes labeled with PKH26 were injected into the tail vein of WT mice. After 24 h, we used IF to assess the B16/F10-derived exosomes in the lungs of WT mice. Our results demonstrated that the B16/F10-derived exosomes were primarily taken up by S100A4$^+$ fibroblasts (Figure 4a). These observations suggest that lung fibroblasts might be involved in recruiting MDSCs required for pre-metastatic microenvironment formation. Furthermore, the in vitro experimental results revealed that the fibroblasts treated with the exosomes activated S100A10 expression (Figure 4b) and the expression of a series of chemokine genes, including CCL2, CXCL1, CXCL2, CXCL5 and CXCL8 (Figure 4c). The number of MDSCs that migrated in response to B16/F10 exosome-stimulated fibroblasts conditioned medium (FCM) was four times greater than with FCM alone (Figure 4d). These data suggest that fibroblasts, exposed to B16/F10-derived exosomes, activate chemokines expression in order to induce MDSCs migration.

To test which chemokines are regulated by S100A10, we knocked down S100A10 (Figure 4e) and measured chemokine expression. B16/F10-derived exosomes induced the expression of CXCL1 and CXCL8 but not in the fibroblasts of S100A10 deficient (Figure 4f). Meanwhile, the B16/F10 exosome-stimulated conditioned medium of S100A10 deficient fibroblasts reduced the ability to induce migration of MDSCs compared to WT FCM (Figure 4g). Furthermore, we collected fibroblasts treated with the recombinant protein S100A10 and measured

---

MDSCs and M-MDSCs in the lungs of KO or WT mice after B16/F10-derived exosome inoculation was measured via flow cytometry ($n = 6$ individual mice in each group, *$p < 0.05$, **$p < 0.01$). c) The proportion of CD3$^+$CD4$^+$ or CD3$^+$CD8$^+$ T cells in the lungs of KO or WT mice after B16/F10-derived exosome inoculation was measured by flow cytometry ($n = 6$ individual mice in each group, *$p < 0.05$, **$p < 0.01$). d) Immunofluorescent analysis of Gr-1$^+$ cells in WT or KO mice lung sections after B16/F10-derived exosome inoculation (blue-DAPI, green-Gr-1, Scale bar, 25 μm). e) Model diagram of the co-culture system of the T cell, S100A10$^{-/-}$ MDSCs, and S100A10$^{+/+}$ MDSCs. f) Representative images of CFSE-base proliferation assay of T cells co-cultured with S100A10$^{-/-}$ MDSCs and S100A10$^{+/+}$ MDSCs by flow cytometry. g) Quantitative T cell proliferation analysis after co-cultured with S100A10$^{-/-}$ MDSCs and S100A10$^{+/+}$ MDSCs. h) The ARG1, iNOS, and IDO expression of S100A10$^{-/-}$ and S100A10$^{+/+}$ MDSCs in the lung pre-metastatic microenvironment were quantified by qPCR. i) Anti-Gr-1 Abs or isotype control was injected into the tail-vein of WT and KO mice at 200 μg/mouse the day before the B16/F10^{LUC} were implanted. Subsequently, Gr-1 Abs or isotype control was injected every 3 d into tail veins of WT and KO mice. B16/F10 lung metastasis was monitored via luciferase bioluminescence in vivo.
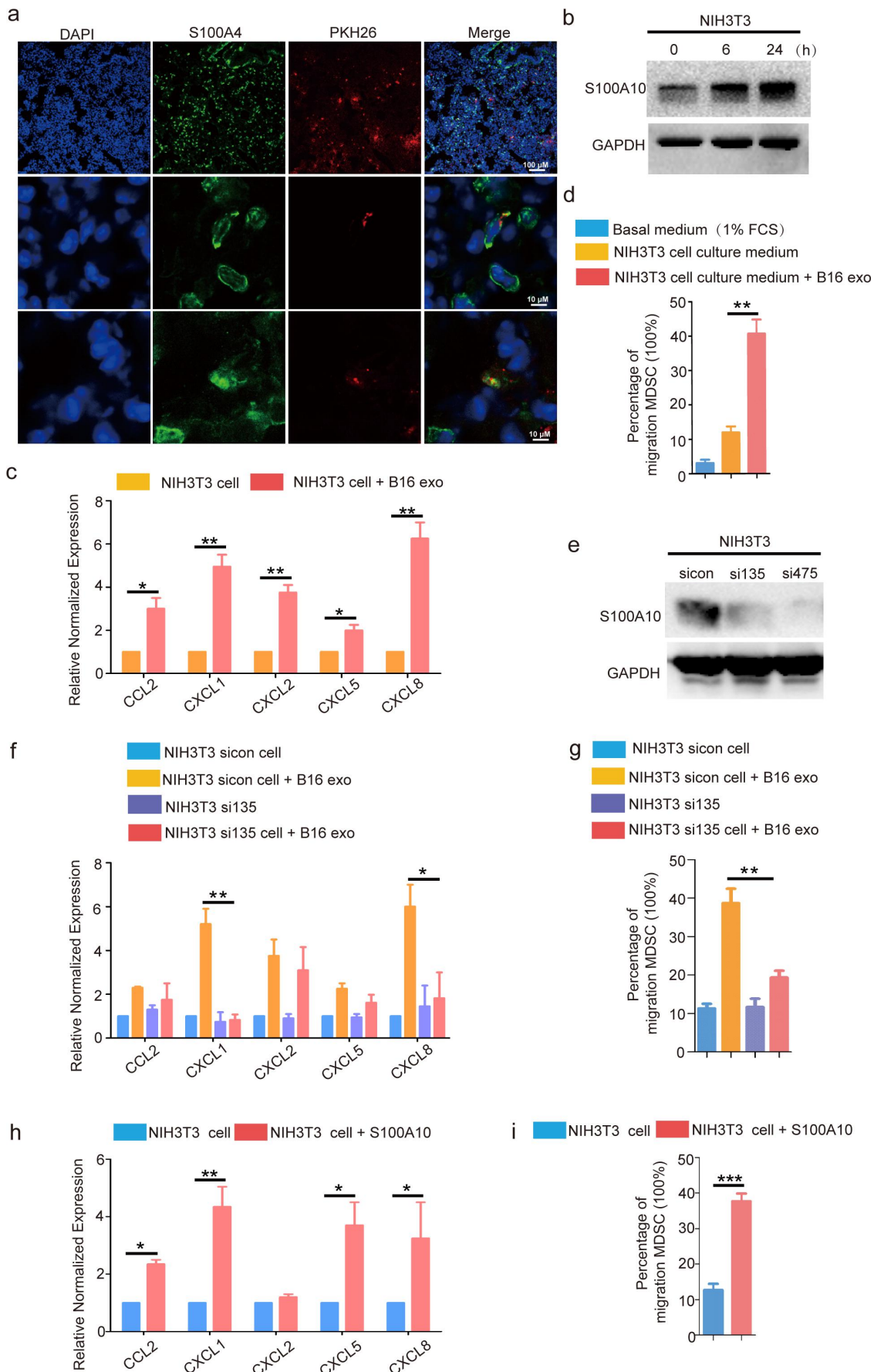
Figure 4. The S100A10 of lung fibroblasts activates CXCL1/CXCL8 expression and increases the migration of myeloid lineage via B16/F10-derived exosome induction. a) Immunofluorescent analysis of the location of S100A4[+] fibroblast and PKH26 marked B16/F10-derived exosome in the lungs of WT mice. b) S100A10 expression in NIH3T3 fibroblast cells stimulated with B16/F10-derived exosomes was detected via immunoblot. c) Chemokine gene expression in NIH3T3 fibroblast cells after B16-derived exosome induction was quantified by qPCR ($n = 6$ individual cells in each group, *$p < 0.05$, **$p < 0.01$). d) Numbers of MDSCs migrating in response to B16/F10 exosome-stimulated fibroblasts conditioned medium (FCM) ($n = 6$ individual cells in each group, **$p < 0.01$). e) S100A10 gene knockdown efficiency in NIH3T3 fibroblast

chemokine expression. The expression of CCL2, CXCL1, CXCL5, and CXCL8 was significantly activated after S100A10 stimulation (Figure 4h), while FCM stimulated with the S100A10 recombinant protein increased induction of MDSCs migration (Figure 4i). These results suggest that the S100A10 of lung fibroblasts participated in MDSCs recruitment during the remodeling of the local immune microenvironment.

Upregulation of lung fibroblasts S100A10 promotes cancer metastasis in vivo

To examine the role of lung fibroblasts S100A10 in cancer metastasis in mice models, we intratracheally delivered adeno-associated virus serotype AAV6-NC or specifically over-expressed S100A10 virus serotype AAV6-S100A10 in lung fibroblasts to WT and KO mice (Figure 5a). At 3 weeks after AAV6 delivery, we harvested lung tissues for analysis and found that S100A10 in lung fibroblasts of AAV6-S100A10 group were significantly higher than those in lung tissue of the AAV6-NC group (Figure 5b-e). At 4 weeks after AAV6 delivery, we injected B16/F10[LUC] into the tail-vein of AAV6-NC group and AAV6-S100A10 group. Compared to AAV6-NC group of KO mice, AAV6-S100A10 group of KO mice increased the cancer metastasis as assessed by bioluminescent (Figure 5f). Furthermore, upregulation of S100A10 in lung fibroblasts promoted the MDSCs recruitment to the lung tissue (Figure 5g,h). Together, these results suggest that upregulation of S100A10 in lung fibroblasts promoted the MDSC recruitment and cancer metastasis in vivo.

S100A10 inhibitor prevents cancer metastasis

Our results indicated that S100A10 plays an important role in cancer metastasis. To test whether the S100A10 inhibitor reduced cancer metastasis, an S100A10 inhibitor was intraperitoneally injected into mice treated with B16/F10 cells. 1-substituted 4-aroyl-3-hydroxy-5-phenyl-1 H-pyrrol-2(5 H)-ones, an effective blocker of S100A10 and AnxA2 binding inhibited the function of S100A10.[22] The Figure 6a shows the chemical structures of the S100A10 inhibitor. We found that treatment with 30 mg/kg/d of the S100A10 inhibitor reduced the number of metastatic nodules (Figure 6b) as well as the weight of the lung tissue (Figure 6c). The HE staining of the whole lung tissue revealed that the cancer metastasis in the inhibitor-treated mice is less than that of the control mice (Figure 6d). The S100A10 inhibitor, 1-Substituted 4-Aroyl-3-hydroxy-5-phenyl-1 H-pyrrol-2(5 H)-one, inhibits lung metastasis. Our findings may aid in the design of new therapeutic targets for cancer metastasis.

In summary, we show that the activation of S100A10 in lung fibroblasts via tumor-derived exosomes initiates MDSCs recruitment and remodels the local immune microenvironment during

cancer metastasis (Figure 6e). Therefore, S100A10 of host interstitial cells is a potent inducing factor during lung metastasis.

Discussion

Previous studies on cancer metastasis have suggested complex interactions facilitated by cancer, BMDCs, and immune cells. Moreover, recent studies have highlighted the pleiotropic functions of MDSCs by promoting distant metastasis via inflammation and immunosuppression. MDSCs through the secretion of inflammatory cytokines and growth factors remodel the local microenvironment, resulting in the colonization and growth of cancer cells. Experimental evidence suggests that MDSCs are abundant in the pre-metastatic lung and are related to the burden of subsequent metastatic breast cancer.[23] MDSCs, mobilized with G-CSF in distant organs before the arrival of in situ tumor cells, produces the Bv8 protein in order to stimulate the migration of breast cancer cells.[24] Furthermore, MDSCs facilitate metastatic growth via the induction of vascular leakage and the remodeling of ECM, as well as systemic effects on the immune system.[5,6,24] Interestingly, in our study, we found that S100A10 deficiency reduced MDSCs accumulation during the remodeling of the local immune microenvironment of the lungs. Our results suggest that S100A10 deficiency affects MDSCs recruitment and cancer metastasis. Previous studies on the function of S100A10 on the recruitment of immune cells into the primary tumor microenvironment have revealed that S100A10 regulates the migration of macrophages to the tumor sites.[25,26] The function of the S100A10 plasminogen receptor could partially explain this. S100A10 binding to plasminogen results in the conversion of plasminogen to plasmin via the activation of plasminogen activators-tissue-type plasminogen activator (t-PA) and urokinase-type-plasminogen activator (uPA).[26,27] The plasminogen activation process is integral to macrophage migration under inflammatory stimulation.[28–30] In the S100A10 deficient mice lung immune microenvironment, the macrophage cells did not reveal any differences compared to WT mice. This may illustrate the different roles of S100A10 during the formation of the primary tumor microenvironment and cancer metastasis.

Lung fibroblasts have functional plasticity during promoting local immune microenvironment formation.[31] The COX-2^{+} lung fibroblasts improve lung-resident myeloid cells' immune-suppressive function and drive dysfunctional dendritic cells, resulting in increased immunosuppression and lung metastasis in breast cancer models.[32] TDFS acts on the lung fibroblasts that are activated by the p38α kinase/type I interferon signaling/fibroblast activation protein axis, resulting in the remodeling of the ECM in the lungs.[33] In our WT mice model, lung fibroblast cells primarily take up exosomes derived from B16/F10 cells.

---

cells was detected via immunoblot. f) Chemokine gene expression in S100A10 knockdown NIH3T3 fibroblast cells after B16-derived exosome induction was quantified via qPCR (n = 6 individual cells in each group, *p < 0.05, **p < 0.01). g) Numbers of MDSCs migrating in response to B16/F10 exosome-stimulated S100A10 knockdown NIH3T3 fibroblasts conditioned medium (n = 6 individual cells in each group, **p < 0.01). h) Chemokine gene expression in NIH3T3 fibroblast cells after S100A10 recombinant protein induction was quantified via qPCR (n = 6 individual cells in each group, *p < 0.05, **p < 0.01). i) Numbers of MDSCs migrating in response to the recombinant protein S100A10 stimulated NIH3T3 fibroblasts conditioned medium (n = 6 individual cells in each group, ***p < 0.001).
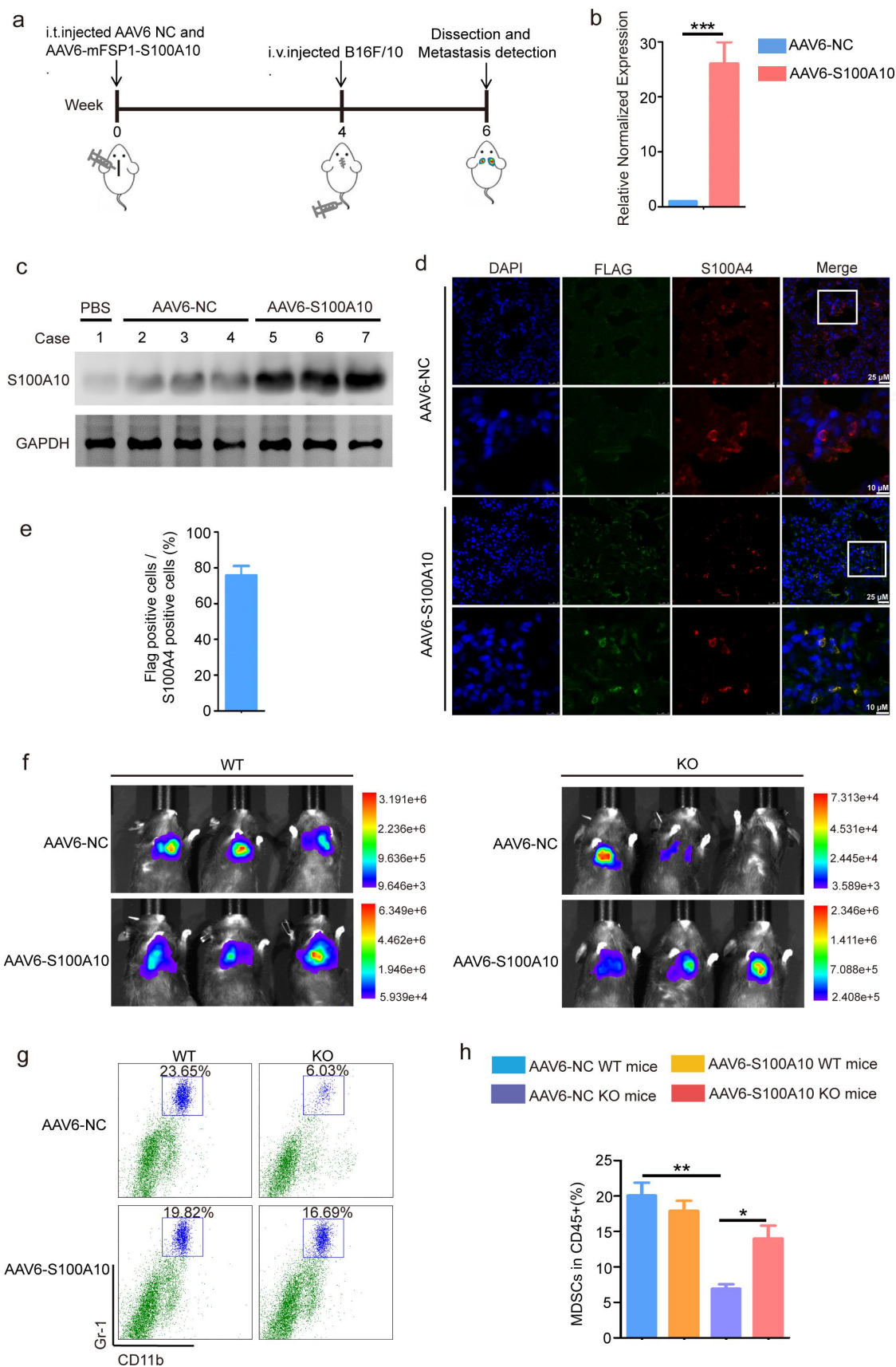
Figure 5. Upregulation of S100A10 expression in lung fibroblasts promotes lung metastasis of tumor in KO mice. a) The schematic diagram for AAV6-NC or AAV6-S100A10 infection in the lungs of WT and KO mice. Six-week-old WT and KO mice were intratracheally injected with AAV6-NC and AAV6-S100A10. Four weeks after AAV administration, the B16/F10^{LUC} cells were injected into the tail-vein of WT and KO mice. Two weeks after the B16/F10^{LUC} cells were injected, tumor metastasis was assessed via luciferase bioluminescence in vivo. b) qRCR analysis of S100A10 mRNA expression in the lungs of mice from the AAV6-NC and AAV6-S100A10 groups ($n = 6$ individual cells in each group, ***$p < 0.001$). c) Western blot analysis of S100A10 expression in the lungs of mice from the AAV6-NC and AAV6-S100A10 groups ($n = 3$ per group). d) Immunofluorescence staining with S100A4$^+$ fibroblasts and Flag-marked fibroblast-specific AAV6-S100A10 in the lungs of WT mice. e) Statistical analysis of the percent of AAV6-S100A10 transduction in S100A4$^+$ fibroblasts ($n = 3$ mice, five fields assessed per mouse). f) Representative luciferase bioluminescence images of B16/F10 lung metastasis in WT or KO mice via AAV6-NC and AAV6-S100A10 infection. g and h) The proportion of MDSCs in the lungs of KO or WT mice after AAV6-NC and AAV6-S100A10 infection was measured via flow cytometry ($n = 6$ individual mice in each group, *$p < 0.05$, **$p < 0.01$).
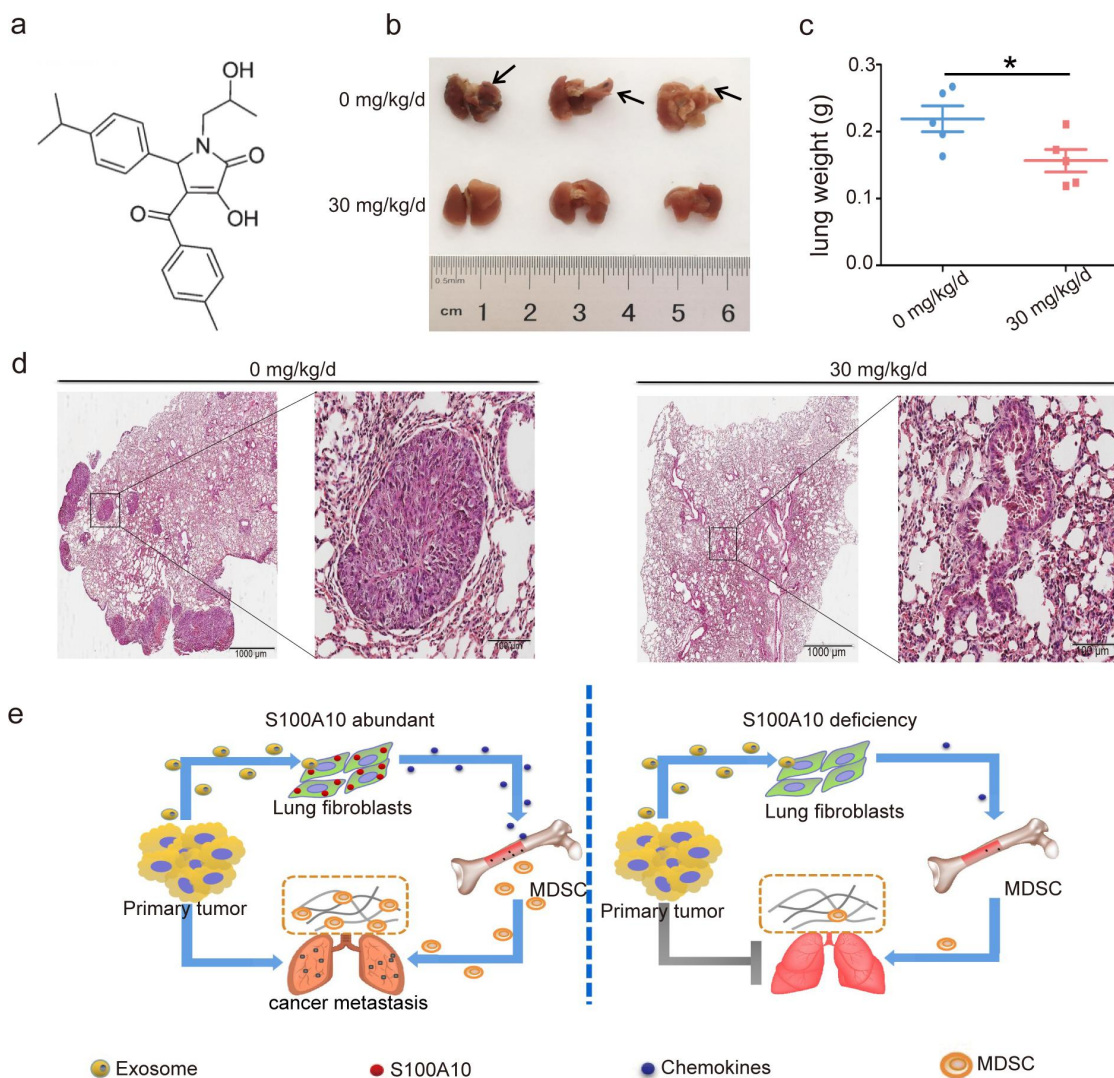
Figure 6. S100A10 inhibitor prevents lung metastasis. a) Chemical structures of the S100A10 inhibitor 1-substituted 4-aroyl-3-hydroxy-5-phenyl-1 H-pyrrol-2(5 H)-ones. b) Representative images of B16/F10 lung metastasis nodules of C57 mice in treated with vehicle or S100A10 inhibitor 30 mg/kg/d via BFI. c) In vivo quantitation of B16/F10 metastasis lung weight of C57 mice treated with vehicle or S100A10 inhibitor 30 mg/kg/d ($n = 5$ individual mice in each group, $*p < 0.05$). d) H&E-stained lung sections of C57 mice treated with vehicle or S100A10 inhibitor 30 mg/kg/d. e) Schematic activation model of S100A10 in host lung fibroblast cells via tumor exosome initiated MDSCs recruitment promotes lung pre-metastatic microenvironment formation and cancer metastasis.

Subsequently, the expression of S100A10 and the important chemokines CCL2, CXCL1, CXCL2, CXCL5, and CXCL8 were significantly activated in lung fibroblasts. However, B16/F10-derived exosomes cannot induce the expression of CXCL1 and CXCL8 in the S100A10 deficient fibroblasts. Increased expression of CXCL1 and CXCL8 is commonly seen in many tumors,[34–37] The up-regulated CXCL1 and CXCL8 reflect high tumor burden, poor tumor differentiation, and poor prognosis.[38,39] The function of the CXCL1 and CXCL8 is chemotactic for MDSCs, neutrophils, and monocytes and remodels the immune microenvironment of the tumor. In co-implantation experiments, the growth of xenograft tumors was increased with MDSCs from CXCL8 transgenic mice as compared to MDSCs from WT mice.[40] Tumor-derived CXCL8 showed increased mobilization of MDSCs into the tumor site.[40,41] In CXCR2$^{-/-}$ mice, CXCL1/2/5-CXCR2 signaling led to the recruitment of MDSCs into the liver.[42] These results indicate that CXCL1 and CXCL8 are important chemokines that cause immune cells infiltration into the local immune microenvironment. We found that S100A10 deficiency of lung fibroblasts inhibited the activation of CXCL1 and CXCL8. Meanwhile, tumor-derived exosomes induced migration of myeloid lineage was decreased. In particular, we found that the S100A10 recombinant protein significantly activated fibroblast CXCL1 and CXCL8 expression of and induced the migration of the myeloid lineage. We propose that S100A10 contributes to the promotion of MDSCs recruitment and pre-metastatic microenvironment formation by inducing the activation of CXCL1 and CXCL8 in lung fibroblasts. This study highlighted the vital role of S100A10 in driving MDSCs recruitment into the lungs as an early step of primary cancer metastasis.

Acknowledgments

Disclosure statement

The authors declare that they have no known competing financial interests or personal relationships.

Funding

ORCID

Peijun Liu 🔟 http://orcid.org/0000-0003-0529-387X

Data availability statement

The data that support the findings of this study are available from the corresponding author upon reasonable request.

References

1. Quail DF, Joyce JA. Microenvironmental regulation of tumor progression and metastasis. Nat Med. 2013;19:1423–1437.
2. Han L, Lam EW-F, Sun Y. Extracellular vesicles in the tumor microenvironment: old stories, but new tales. Mol Cancer. 2019;18(1):59. doi:10.1186/s12943-019-0980-8.
3. Wortzel I, Dror S, Kenific CM, Lyden D. Exosome-mediated metastasis: communication from a distance. Dev Cell. 2019;49 (3):347–360. doi:10.1016/j.devcel.2019.04.011.
4. Nakamura K, Smyth MJ. Myeloid immunosuppression and immune checkpoints in the tumor microenvironment. Cell Mol Immunol. 2020;17(1):1–12. doi:10.1038/s41423-019-0306-1.
5. Kumar V, Patel S, Tcyganov E, Gabrilovich DI. The nature of myeloid-derived suppressor cells in the tumor microenvironment. Trends Immunol. 2016;37(3):208–220. doi:10.1016/j.it.2016.01.004
6. Hua BL, Garstka MA, Li ZF. Chemokines and their receptors promoting the recruitment of myeloid -derived suppressor cells into the tumor. Mol Immunol. 2020;117:201–215. doi:10.1016/j.molimm.2019.11.014.
7. Veglia F, Perego M, Garbrilovich D. Myeloid-derived suppressor cells coming of age. Nat Immunol. 2018;19(2):108–119. doi:10.1038/s41590-017-0022-x.
8. Davidson S, Coles M, Thomas T, Kollias G, Ludewig B, Turley S, Brenner M, Buckley CD. Fibroblasts as immune regulators in infection, inflammation and cancer. Nat Rev Immunol. 2021;21 (11):704–717. doi:10.1038/s41577-021-00540-z.
9. Desbois M, Wang Y. Cancer-associated fibroblasts: key players in shaping the tumor immune microenvironment. Immunol Rev. 2021;302(1):241–258. doi:10.1111/imr.12982.
10. Miller VA, Madureira PA, Kamaludin AA, Komar J, Sharma V, Sahni G, Thelwell C, Longstaff C, Waisman DM. Mechanism of plasmin generation by S100A10. Thromb Haemost. 2017;117 (06):1058–1071. doi:10.1160/TH16-12-0936.
11. Yang X, Popescu NC, Zimonjic DB. DLC1 interaction with S100A10 mediates inhibition of in vitro cell invasion and tumorigenicity of lung cancer cells through a RhoGAP-independent mechanism. Cancer Res. 2011;5(8):2916–2925. doi:10.1158/0008-5472.CAN-10-2158.
12. Zhou X, Shi M, Cao J, Yuan T, Yu G, Chen Y, Fang W, Li H. S100 calcium binding protein A10, a novel oncogene, promotes the proliferation, invasion, and migration of hepatocellular carcinoma. Front Genet. 2021;12:695036. doi:10.3389/fgene.2021.695036.
13. Svenningsson P, Chergui K, Rachleff I, Flajolet M, Zhang X, El Yacoubi M, Vaugeois J-M, Nomikos GG, Greengard P. Alterations in 5-HT 1B receptor function by p11 in Depression-Like States. Science. 2006;311(5757):77–80. doi:10.1126/science.1117571.
14. van de Graaf SF, Hoenderop JG, Gkika D, Lamers D, Prenen J, Rescher U, Gerke V, Staub O, Nilius B, Bindels RF. Functional expression of the epithelial Ca(2+) channels (TRPV5 and TRPV6) requires association of the S100A10-annexin 2 complex. Embo J. 2003;22:1478–1487. doi:10.1093/emboj/cdg162.
15. Okuse K, Malik-Hall M, Baker MD, Poon WY, Kong H, Chao MV, Wood JN. Annexin II light chain regulates sensory neuron-specific sodium channel expression. Nature. 2002;417(6889):653–656. doi:10.1038/nature00781.
16. Lu H, Xie Y, Tran L, Lan J, Yang Y, Murugan NL, Wang R, Wang YJ, Semenza GL. Chemotherapy-induced S100A10 recruits KDM6A to facilitate OCT4-mediated breast cancer stemness. J Clin Invest. 2020;130(9):4607–4623. doi:10.1172/JCI138577.
17. Eisenblaetter M, Flores-Borja F, Lee JJ, Wefers C, Smith H, Hueting R, Cooper MS, Blower PJ, Patel D, Rodriguez-Justo M. et al. Visualization of tumor-immune interaction-target-specific imaging of S100A8/A9 reveals pre-metastatic niche establishment. Theranostics. 2017;7(9):2392–2401. doi:10.7150/thno.17138.
18. Lukanidin E, Sleeman JP. Building the niche: the role of the S100 proteins in metastatic growth. Semin Cancer Biol. 2012;22(3):216–225. doi:10.1016/j.semcancer.2012.02.006.
19. Rao VS, Gu Q, Tzschentke S, Lin K, Ganig N, Thepkaysone ML, Wong FC, Polster H, Seifert L, Seifert AM. et al. Extravesicular TIMP-1 is a non-invasive independent prognostic marker and potential therapeutic target in colorectal liver metastases. Oncogene. Oncogene. 2022;41(12):1809–1820. doi:10.1038/s41388-022-02218-9.
20. Hiratsuka S, Watanabe A, Sakurai Y, Akashi-Takamura S, Ishibashi S, Miyake K, Shibuya M, Akira S, Aburatani H, Maru Y. et al. The S100A8–serum amyloid A3–TLR4 paracrine cascade establishes a pre-metastatic phase. Nat Cell Biol. 2008;10 (11):1349–1355. doi:10.1038/ncb1794.
21. Sara F, Santos L, Sampaio-Ribeiro G, Ferreira HR, Lima N, Caetano R, Abreu M, Zuzarte M, Ribeiro AS, Paiva A. et al. Unveiling the role of osteosarcoma-derived secretome in premetastatic lung remodelling. J Exp Clin Cancer Res. 2023;42(1):328. doi:10.1186/s13046-023-02886-9.
22. Reddy TR, Li C, Guo X, Myrvang HK, Fischer PM, Dekker LV. Design, synthesis, and Structure–Activity relationship exploration of 1-substituted 4-aroyl-3-hydroxy-5-phenyl-1 H -pyrrol-2(5 H)-one Analogues as inhibitors of the annexin A2–S100A10 protein interaction. J Med Chem. 2011;54(7):2080–2094. doi:10.1021/jm101212e.
23. Monteran L, Ershaid N, Doron H, Zait Y, Scharff Y, Ben-Yosef S, Avivi C, Barshack I, Sonnenblick A, Erez N. et al. Chemotherapy-induced complement signaling modulates immunosuppression and metastatic relapse in breast cancer. Nat Commun. 2022;13 (1):5797. doi:10.1038/s41467-022-33598-x.
24. Kowanetz M, Wu X, Lee J, Tan M, Hagenbeek T, Qu X, Yu L, Ross J, Korsisaari N, Cao T. et al. Granulocyte-colony stimulating factor promotes lung metastasis through mobilization of Ly6G+Ly6C+ granulocytes. Proc Natl Acad Sci USA. 2010;107(50):21248–21255. doi:10.1073/pnas.1015855107.
25. Sceneay J, Parker BS, Smyth MJ, Moller A. Hypoxia-driven immunosuppression contributes to the pre-metastatic niche. Oncoimmunology. 2013;2(1):e22355. doi:10.4161/onci.22355.
26. Phipps KD, Surette AP, Pa O, Waisman DM. Plasminogen receptor S100A10 is essential for the migration of tumor-promoting macrophages into tumor sites.Cancer res. 2011;71(21):6676–6683. doi:10.1158/0008-5472.CAN-11-1748.
27. O'Connell PA, Surette AP, Liwski RS, Svenningsson P, Waisman DM. Waisman DM.S100A10 regulates plasminogen-dependent

macrophage invasion. Blood. 2010;116(7):1136–1146. doi:10.1182/blood-2010-01-264754.

28. Surette AP, Madureira PA, Phipps KD, Miller VA, Svenningsson P, Waisman DM. Regulation of fibrinolysis by S100A10 in vivo. Blood. 2011;118(11):3172–3181. doi:10.1182/blood-2011-05-353482.

29. Kubala MH, Punj V, Placencio-Hickok VR, Fang H, Fernandez GE, Sposto R, DeClerck YA. Plasminogen activator inhibitor-1 promotes the recruitment and polarization of macrophages in cancer. Cell Rep. 2018;25(8):2177–2191. doi:10.1016/j.celrep.2018.10.082.

30. Sugimoto MA, Ribeiro ALC, Costa BRC, Vago JP, Lima KM, Carneiro FS, Ortiz MMO, Lima GLN, Carmo AAF, Rocha RM. et al. Plasmin and plasminogen induce macrophage reprogramming and regulate key steps of inflammation resolution via annexin A1. Blood. 2017;129(21):2896–2907. doi:10.1182/blood-2016-09-742825.

31. Gong Z, Li Q, Shi J, Wei J, Li P, Chang CH, Shultz LD, Ren G. Lung fibroblasts facilitate pre-metastatic niche formation by remodeling the local immune microenvironment. Immunity. 2022;55(8):1483–1500. doi:10.1016/j.immuni.2022.07.001.

32. Zhang H, Jiang H, Zhu L, Li J, Ma S. Cancer-associated fibroblasts in non-small cell lung cancer: recent advances and future perspectives. Cancer Lett. 2021;514:38–47. doi:10.1016/j.canlet.2021.05.009.

33. Gui J, Zahedi F, Ortiz A, Cho C, Katlinski KV, Alicea-Torres K, Li J, Todd L, Zhang H, Beiting DP. et al. Activation of p38α stress-activated protein kinase drives the formation of the pre-metastatic niche in the lungs. Nat Cancer. 2020;1(6):603–619. doi:10.1038/s43018-020-0024-0.

34. Wang D, Sun H, Wei J, Cen B, DuBois RN. CXCL1 is critical for premetastatic niche formation and metastasis in colorectal cancer. Cancer Res. 2017;77(13):3655–3665. doi:10.1158/0008-5472.CAN-16-3199.

35. Su L, Li N, Tang H, Lou Z, Chong X, Zhang CG, Su J, Dong X. Kupffer cell-derived TNF-α promotes hepatocytes to produce CXCL1 and mobilize neutrophils in response to necrotic cells. Cell Death Dis. 2018;9(3):323. doi:10.1038/s41419-018-0377-4.

36. Ha H, Debnath B. Neamati N.Role of the CXCL8-CXCR1/2 axis in cancer and inflammatory diseases. Theranostics. 2017;7(6):1543–1588. doi:10.7150/thno.15625.

37. Liu Q, Li A, Tian Y, Wu JD, Liu Y, Li T, Chen Y, Han X, Wu K. The CXCL8-CXCR1/2 pathway in cancer. Cytokine Growth Factor Rev. 2016;3:61–71. doi:10.1016/j.cytogfr.2016.08.002.

38. Cacev T, Radosevic S, Krizanac S, Kapitanovic S. Kapitanovic S. Influence of interleukin-8 and interleukin-10 on sporadic colon cancer development and progression. Carcinogenesis. 2008;29(8):1572–1580. doi:10.1093/carcin/bgn164.

39. Highfill SL, Cui Y, Giles AJ, Smith JP, Zhang H, Morse E, Kaplan RN, Mackall CL. Disruption of CXCR2-mediated MDSCs tumor trafficking enhances anti-PD1 efficacy. Sci Transl Med. 2014;6(237):237–267. doi:10.1126/scitranslmed.3007974.

40. Asfaha S, Dubeykovskiy AN, Tomita H, Yang X, Stokes S, Shibata W, Friedman RA, Ariyama H, Dubeykovskaya ZA, Muthupalani S. et al. Mice that express human interleukin-8 have increased mobilization of immature myeloid cells, which exacerbates inflammation and accelerates colon carcinogenesis. Gastroenterology. 2013;144(1):155–166. doi:10.1053/j.gastro.2012.09.057.

41. David JM, Dominguez C, Hamilton DH, Palena C. The IL-8/IL-8R axis: a double agent in tumor immune resistance. Vaccines. 2016;4(3):22. doi:10.3390/vaccines4030022.

42. Katoh H, Wang D, Daikoku T, Sun H, Dey SK, Dubois RN. CXCR2-expressing myeloid-derived suppressor cells are essential to promote colitis-associated tumorigenesis. Cancer Cell. 2013;24(5):631–644. doi:10.1016/j.ccr.2013.10.009.